Interplanetary Coronal Mass Ejections and Stream Interaction Regions Observed by Tianwen-1 and MAVEN at Mars

Yutian Chi[1] , Chenglong Shen[2,3] , Long Cheng[4] , Bingkun Yu[1] , Bin Miao[2,3], Yuming Wang[2,3,5] , Tielong Zhang[6,7],
Zhuxuan Zou[4] , Mengjiao Xu[1] , Zonghao Pan[2,3], Zhenpeng Su[2,3] , Jingnan Guo[2,3], Dongwei Mao[4], Zhihui Zhong[4] ,
Zhiyong Zhang[4], Junyan Liu[4] , Can Wang[4], Zhiyong Wu[4], Guoqiang Wang[7], Sudong Xiao[7], Kai Liu[2,3] , Xinjun Hao[2,3],
Yiren Li[2,3], Manming Chen[2,3], and Yang Du[8]

[1] Institute of Deep Space Sciences, Deep Space Exploration Laboratory, Hefei 230088, People's Republic of China
[2] Deep Space Exploration Laboratory/School of Earth and Space Sciences, University of Science and Technology of China, Hefei 230026, People's Republic of China; clshen@ustc.edu.cn
[3] CAS Center for Excellence in Comparative Planetology, University of Science and Technology of China, Hefei, People's Republic of China
[4] CAS Key Laboratory of Geospace Environment, Department of Geophysics and Planetary Sciences, University of Science and Technology of China, Hefei, People's Republic of China
[5] Anhui Mengcheng Geophysics National Observation and Research Station, University of Science and Technology of China, Mengcheng, Anhui, People's Republic of China
[6] Space Research Institute, Austrian Academy of Sciences, Graz, Austria
[7] Institute of Space Science and Applied Technology, Harbin Institute of Technology, Shenzhen, People's Republic of China
[8] Shanghai Institute of Satellite Engineering, Shanghai, People's Republic of China

Abstract

The Tianwen-1 spacecraft is China's first Mars exploration mission. The Mars Orbiter Magnetometer (MOMAG) is a scientific instrument on board the Tianwen-1 mission that is designed to study magnetic fields at Mars, including the solar wind to the magnetosheath and the ionosphere. Using the first Tianwen-1/MOMAG data that is publicly available, we present an interplanetary coronal mass ejection (ICME) and stream interaction region (SIR) list based on in situ observations at Mars between 2021 November 16 and 2021 December 31. We compared the magnetic field intensity and vector magnetic field measurements from Tianwen-1/MOMAG and Mars Atmospheric Volatile EvolutioN (MAVEN)/Magnetometer (MAG) during the ICME and SIR interval and found a generally good consistency between them. Due to MAVEN's orbital adjustment since 2019, the Tianwen-1/MOMAG instrument is almost unique in its status as an interplanetary magnetic field monitor currently at Mars. The observations indicate that the MOMAG instrument on Tianwen-1 is performing well and can provide accurate measurements of the vector magnetic field in the near-Mars solar wind space. The multipoint observations combining MOMAG, MINPA, and MEPA on board Tianwen-1 with MAG, SWIA, and STATIC on board MAVEN will help develop systematic studies of the characteristics of ICMEs and SIRs at Mars, and their influences on the Martian atmosphere and ionosphere.

1. Introduction

Coronal mass ejections (CMEs) and stream interaction regions (SIRs) are the two most common large-scale disturbances in the heliosphere, driving extreme space weather in Earth's and other planetary environments (Gonzalez et al. 1999; Crider et al. 2005; Richardson & Cane 2012; Zhang et al. 2021b). CMEs are the large-scale eruptions of plasma and magnetic flux, transferring huge energies from the lower solar corona into interplanetary space. Interplanetary CMEs (ICMEs) are the major cause of severe space weather, especially around the solar maximum (Zhang et al. 2007; Shen et al. 2017). SIRs are mainly created by the interaction between fast solar wind streams (emanating from coronal holes) and the low-speed streams arising in the streamer belt (Gosling & Pizzo 1999). If SIRs persist for more than one solar rotation, they can also be referred to as corotating interaction regions (Jian et al. 2006). At Earth, ICMEs can cause intense geomagnetic storms (Zhang

et al. 2021b), extensive ionospheric anomalies (Wang et al. 2016), and disturbances in the atmosphere–ionosphere coupling system (Yiğit et al. 2016), and trigger a wide array of undesirable consequences, including disruption in satellite systems, damage to ground-based electric power grids, and interruptions of high-frequency communications and satellite navigation systems (Cannon et al. 2013). SIRs passing the Earth can cause recurrent geomagnetic storms (Chi et al. 2018), change the energetic particle environment near Earth (Rouillard & Lockwood 2007), and produce periodic oscillations in the ionosphere (Yu et al. 2021).

In contrast to Earth, Mars lacks global intrinsic magnetic fields but possesses localized crustal fields (Connerney et al. 2015b). Thus, the ICMEs/SIRs carry the interplanetary magnetic field and have direct access to the Martian atmosphere/ionosphere. Many previous studies used multiple spacecraft in situ observations and numerical simulations to investigate the interaction between solar transient events and Martian atmosphere. During the passage of the solar transient events (ICMEs), the solar wind interaction region was compressed (Crider et al. 2005), and the cold ion escape of the Martian atmospheric rates increased (Brain et al. 2015;

Zhang et al. 2021a), which both indicate that the interaction between ICMEs and Mars is a significant factor in the evolution of the Martian atmosphere (Xu et al. 2018). SIRs can cause strong perturbations in the Martian-induced magnetosphere and ionosphere (Dubinin et al. 2009). The highly energetic particles accelerated by shocks associated with ICMEs and SIRs can also cause an enhancement in the ionospheric ionization (Morgan et al. 2010). The ICMEs/SIRs passing Mars can strongly affect the Martian environment. Studying the in situ characteristics of ICMEs/SIRs at Mars is critical for understanding the evolution of the Martian atmosphere and ionosphere.

The solar wind parameters near Mars have been continuously monitored by Mars Atmosphere and Volatile EvolutioN (MAVEN) since 2014, the Mars Express spacecraft since 2003, and Tianwen-1 since 2021 November. The Tianwen-1 spacecraft (Wan et al. 2020) is China's first Mars exploration mission, launched on 2020 July 23, with a primary mission target of studying environmental characteristics around Mars. The Mars Orbiter Magnetometer (MOMAG; Liu et al. 2020), one of the orbiter's seven payloads, monitors the magnetic fields around Mars to learn more about its space environment and how it interacts with the solar wind. Since 2021 November 16, the MOMAG instrument on board the Tianwen-1 spacecraft has been continuously measuring the local magnetic field conditions around Mars, and its reliability has been verified by Zou et al. (2023). Despite the fact that MAVEN and Tianwen-1 are primarily planetary missions, both spacecraft repeatedly crossed the Martian magnetosphere and spent significant amounts of time in the solar wind, recording huge solar transient structures, such as ICMEs and SIRs. The MAVEN spacecraft (Jakosky et al. 2015a) was launched on 2013 November 18, and has been investigating the interactions of the Sun and the solar wind with the Martian magnetosphere and upper atmosphere for 8 yr. The Magnetometer (MAG; Connerney et al. 2015a) and the Solar Wind Ion Analyzer (SWIA; Halekas et al. 2015) on board MAVEN measure the intensity and direction of the magnetic field, density, temperature, bulk flow velocities, and dynamic pressure around Mars. Instruments on board MAVEN and Tianwen-1 can simultaneously detect the arrival of ICMEs and SIRs. The multipoint observations combining Tianwen-1 and MAVEN provide an opportunity to systematically study the characteristics of ICMEs and SIRs, and their influences on the Martian atmosphere and ionosphere.

In this work, we use the Tianwen-1 and MAVEN in situ observations to identify ICME and SIR events and give a detailed description of those five events. The layout of this paper is as follows. Section 2 briefly describes the in situ magnetic field and solar wind plasma observations from Tianwen-1 and MAVEN, and the criteria to identify ICMEs and SIRs used in this study. In Section 3, we present the first two ICMEs detected by the Tianwen-1 spacecraft, and give a comparison of the magnetic field observations from Tianwen-1 and MAVEN during the two ICMEs. In Section 4, we present the first three SIRs detected by Tianwen-1 and the properties of SIRs near Mars. A summary of our main results and discussion are presented in the final section.

2. Data Set and Criteria

Figure 1 presents the orbits of Mars, Venus, Mercury, STEREO-A, and Earth in Heliocentric Earth Ecliptic
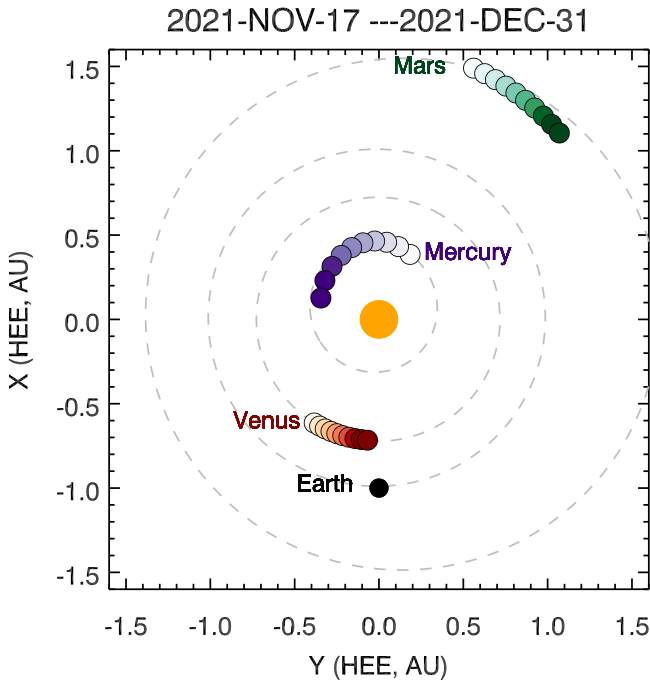
coordinates from 2021 November 16 to 2022 December 31. The orbital tracks are color coded (from light to dark) to represent time (earlier to later). During that time, the Sun-centered longitudinal separation angles of Mars from Earth changed from $\sim$159°3 to 135°9. In this study, we adopt the interplanetary magnetic field vector data from MOMAG on board Tianwen-1 and MAG on board MAVEN, and the solar wind plasma data from MAVEN/SWIA. All the data used in this paper are shown in the Mars Solar Orbital (MSO) coordinate system, with the x-axis pointing from Mars to the Sun, the z-axis aligned with Mars's rotation axis, and the y-axis completing the system.

MAVEN orbits Mars in a $\sim$4.5 hr orbit, while Tianwen-1 orbits Mars in a 7.8 hr orbit. Figure 2 shows the orbits of Tianwen-1 and MAVEN in the period 2021 November 16–18. Tianwen-1 orbits Mars in a steeply inclined elliptical plane with a periapsis of around 1.08 Mars radii (RM) and an apoapsis of about 4.17 RM (red lines in Figure 2). According to Tianwen-1's orbit, the MOMAG spends around 50%–75% of its time in the solar wind, detecting the magnetic field in the solar wind on the dawn–dusk side. MAVEN's orbit plane has a 75° inclination, with a periapsis between 150 and 200 km (1.04–1.06 RM) and an apoapsis between 5900 and 6000 km (2.74–2.77 RM; blue lines in Figure 2). It is apparent that the duration of MOMAG magnetic field data and MAVEN/MAG magnetic field data in the solar wind are different. Thus, considering the differences in the orbits of Tianwen-1 and MAVEN, the observations from MAVEN are complementary to those measured from Tianwen-1. The combination of solar wind measurements from Tianwen-1's and MAVEN's in situ observations will be extremely useful in understanding the characteristics of ICMEs and SIRs at Mars. MAVEN/MAG samples the ambient magnetic field with a sampling frequency of 32 Hz, MAVEN/SWIA has an intrinsic time resolution of 4 s (Halekas et al. 2015), and Tianwen-1/MOMAG samples the magnetic field with a sampling frequency of 1 Hz. As the ICMEs and SIRs are large-scale structures, we use the 10 minutes average data to identify and characterize ICMEs in this work.

The MAVEN and Tianwen-1 spacecraft frequently cross the bow shock. The selection criteria for MAVEN's undisturbed solar wind periods are based on the observations of the solar wind speed $|v| > 200$ km s^{-1}, normalized magnetic field fluctuation levels $\sigma B/|B| < 0.15$ (σB represents a root-sum-squared value of the 32 Hz fluctuation levels in all three components over a 4 s interval), altitude $R > 500$ km, and $\sqrt{(T/|v|)} < 0.012$ (Halekas et al. 2017).

We define the sudden increase in magnetic field intensity as the Tianwen-1 spacecraft crossing the bow shock (Wang et al. 2023). For each orbit, the time Tianwen-1 entered the solar wind from the magnetic sheath and the time the solar wind entered the magnetic sheath can be easily confirmed. The period between the two passes was chosen as Tianwen-1's solar wind period.

Although the signatures of ICMEs can vary significantly, they can still be distinguished from the surrounding solar wind by a particular magnetic field and solar wind plasma signatures. The criteria used to identify ICMEs on Mars are similar to those on Earth (Chi et al. 2016): (1) higher magnetic field strength compared to its surroundings, (2) reasonably monotonic, smooth rotating magnetic field direction, (3) abnormally lower proton temperature, (4) decreasing plasma velocity, and

Figure 1. The orbits of Mars, Venus, Mercury, and Earth in Heliocentric Earth Ecliptic (HEE) coordinates from 2021 November 16 to 2021 December 31, color coded by time. The black dot, red dots, purple dots, and green dots show the position of Earth, Venus, Mercury, and Mars, respectively.

(5) lower plasma beta (β). Please be aware that none of these signatures can be observed in all ICMEs. A structure is recognized as an ICME when it fits at least three of these five criteria. A special type of ICMEs that satisfy the aforementioned five criteria are also called magnetic clouds (MCs; Burlaga et al. 1981). Zhao et al. (2021) identified 24 ICMEs using MAVEN/MAG and SWIA data from 2014 December 6 to 2019 February 21 and presented statistical characteristics of ICMEs at Mars with an average magnetic field strength of 5.99 nT (2.33 ~ 13.23 nT), density of 5.27 cm^{-3} (1.04 ~ 8.59 cm^{-3}), velocity of 394.7 km s^{-1} (331.5 ~ 573.3 km s^{-1}), and dynamic pressure of 1.34 nPa (0.44 ~ 2.96 nPa).

The increasing velocity profile and the significantly enhanced total perpendicular pressure are critical criteria in determining the boundaries of SIRs (Jian et al. 2006; Chi et al. 2018). The compressed and enhanced magnetic field, the increased proton density, and temperature are other important criteria to identify SIRs. Huang et al. (2019) identified 126 SIRs from 2014 October to 2018 November at Mars, and discovered that the average length of SIRs is around 37.0 hr, the mean velocity is 430 km s^{-1}, and the mean maximum magnetic field intensity is 11 nT at 1.5 au.

3. ICME Events

Based on the criteria mentioned in Section 2 and the observations from Tianwen-1/MOMAG and MAVEN/MAG, we identified two ICME events from 2021 November 16 to December 31. Figures 3(a)–(f) show the total magnetic field intensity (B), the elevation (θ), and azimuthal (ϕ) angles of magnetic field direction in the MSO coordinate system; three components of the magnetic field in the MSO coordinate system (B_x, B_y, and B_z) from MAVEN/MAG (black asterisks) and Tianwen-1/MOMAG (red asterisks). As shown in Figure 3, the Tianwen-1/MOMAG magnetic data are

comparable with MAVEN/MAG data. Panels (g)–(l) show the solar wind speed, plasma density, dynamic pressure, proton temperature, total pressure, and plasma beta from MAVEN/SWIA. We only used the plasma and magnetic field data points in the undisturbed solar wind, whose selected criteria are introduced in Section 2.

As indicated by the lavender-colored region in Figure 3, an obvious ICME (ICME-1) was detected near Mars from 00:00 UT on December 10 to 14:10 UT on December 11 lasting about 38 hr. The ICME's front boundary can be well determined, based on the directional discontinuity in the elevation angle θ, and the B_x, B_y, and B_z magnetic field components (panels (b), (d)–(f)). The trailing boundary of the ICME is determined by a sharp enhancement in the plasma density, dynamic pressure, and plasma beta (panels (h), (i) and (l)). The structure exhibits characteristics of a typical ICME including enhanced magnetic field strength, monotonous and smooth-changing magnetic field vector, decreasing velocity, lower plasma density, and lower plasma beta.

According to the MAVEN solar wind selection criteria (Halekas et al. 2015), no undisturbed solar wind data were measured from MAVEN from 06:09 UT to 19:50 UT on 2021 December 10 (indicated by black lines). As shown in Figure 3(j), the plasma temperature during that time is significantly higher than the background solar wind, which might influence the selection of undisturbed solar wind. Thus, for this region, we only use the first three out of four criteria (the solar wind speed $|v| > 200$ km s^{-1}, normalized magnetic field fluctuation levels $\sigma B/|B| < 0.15$, and altitude $R > 500$ km) to select the undisturbed solar wind. The signal of Tianwen-1 across the bow shock is also not noticeable in MOMAG observations during that time. The possible reason is that the arrival of an ICME can dramatically alter the overall morphology of the Martian bow shock (Jakosky et al. 2015b). According to Tianwen-1/MOMAG and MAVEN/MAG observations, ICME-1 has a stronger magnetic field intensity (panel (a)) than the surrounding solar wind. The average magnetic field strengths detected from Tianwen-1/MOMAG and MAVEN/MAG in the interval of ICME-1 are 7.29 nT and 6.74 nT, respectively. In panel (b), the magnetic field elevation angles (θ) from MAG and MOMAG both show distinct rotation from $-90°$ to $90°$. The magnetic field vectors B_x, B_y, and B_z, as shown in panels (d)–(f), from Tianwen-1/MOMAG and MAVEN/MAG rotate simultaneously. According to the rotation of the magnetic field, ICME-1 can also be identified as a south–west–north type MC.

Figure 3 indicates that Tianwen-1/MOMAG is performing well and the magnetic field observations from Tianwen-1/MOMAG and MAVEN/MAG can complement each other. Compared with the typical ICME parameters at Mars studied by Zhao et al. (2021), ICME-1 has a higher magnetic field intensity (7.02 nT), a higher velocity (438.88 km s^{-1}), a lower plasma density (1.82 cm^{-3}), and a lower dynamic pressure (0.57 nPa). Those parameters indicate that ICME-1 corresponds with a strong CME event.

Figure 4 shows the second ICME (ICME-2) detected by the Tianwen-1 and MAVEN spacecraft. An ICME (shown as the lavender-colored shadow) lasted about 44 hr from 00:00 UT on 2021 December 29 to 20:00 UT on 2021 December 30. During this period, the interplanetary observations show obvious ICME signatures with enhanced magnetic field strength, smoothly rotated magnetic field vector, decreasing velocity,

2021-11-16T06:00--2021-11-18T00:00
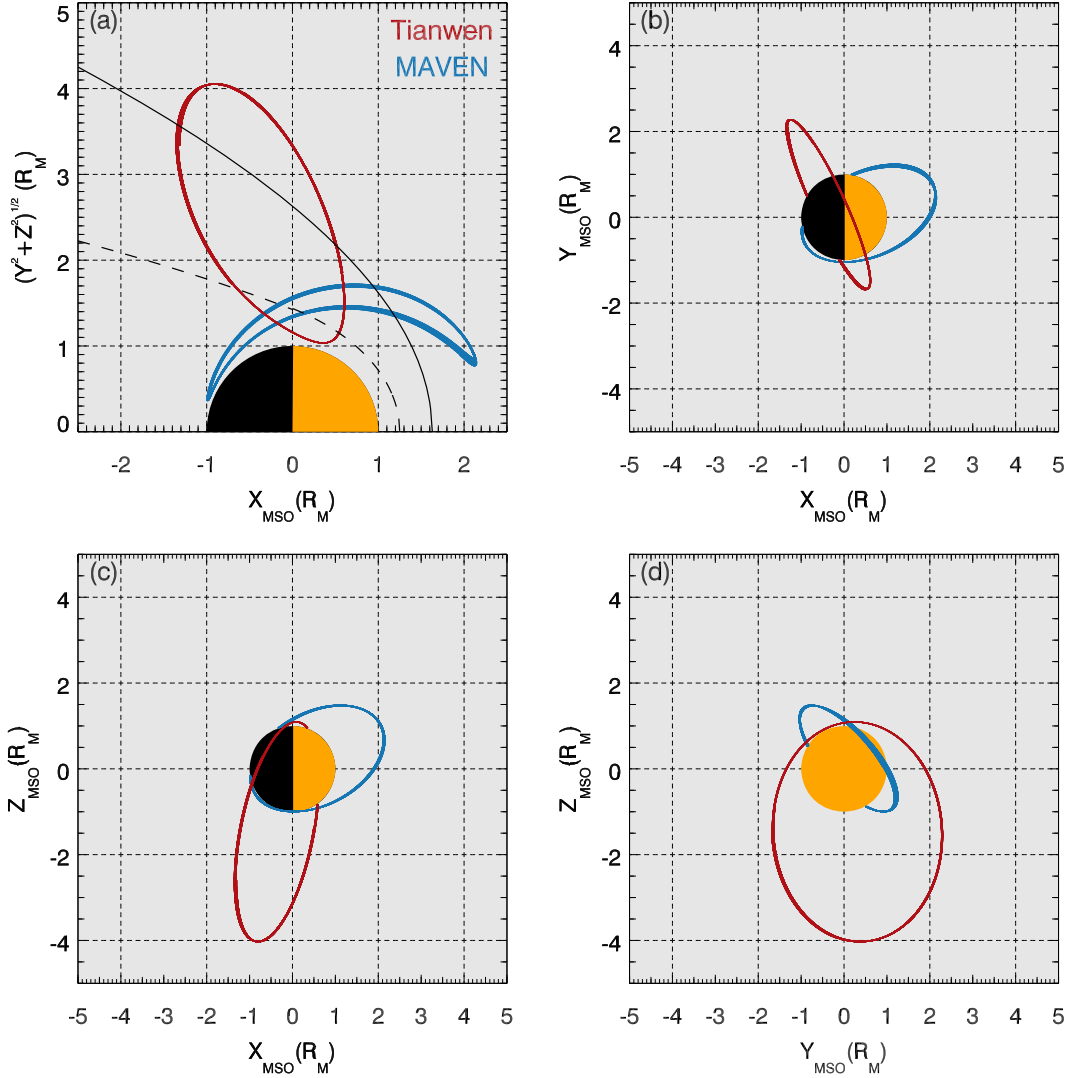
Figure 2. Orbits of Tianwen-1 (red line) and MAVEN (blue line) for the time interval from 06:00 UT on 2021 November 16 to 00:00 UT on 2021 November 18. (a) Tianwen-1's and MAVEN's trajectories in a cylindrical coordinate system. The inner dashed black line indicates the average location of the magnetic pileup boundary, and the outer black line marks the average location of the bow shock (Trotignon et al. 2006). (b) The orbits of the two spacecraft in the X–Y plane along the $Z = 0$ plane. (c) The orbits of the two spacecraft in the X–Z plane along the $y = 0$ plane. The Sun is to the right. (d) The orbits of the two spacecraft as viewed from the Sun. The panels are presented in the MSO coordinate system.

low proton temperature, and lower plasma beta. The data from Tianwen-1/MOMAG in the interval of ICME-2 reveal a comparable magnetic field strength and vector with MAVEN/MAG in panels (d)–(f). During the ICME-2 interval, MAVEN is only in the undisturbed solar wind for a short time, as shown in panels (d)–(f). The Tianwen-1/MOMAG data are crucial for identifying the ICME-2 boundary and displaying the magnetic field direction rotation. ICME-2 has a higher magnetic field intensity (6.33 nT), a lower velocity (335.55 km s^{-1}), a higher plasma density (6.37 cm^{-3}), and comparable dynamic pressure (1.20 nPa) compared with the typical ICME parameters at Mars studied by Zhao et al. (2021). We use a velocity-modified cylindrical force-free flux-rope model (Wang et al. 2015) to fit the two ICME events. The orientation of the fitted flux-rope axis of ICME-1 has a longitude of 284°.61 and a latitude of −17°.35, while that of ICME-2 has a longitude of 299°.61 and a latitude of 54°.34. The expansion velocities for the ICME-1 and ICME-2 are 1.091 km s^{-1} and 0.513 km s^{-1}, respectively. It

indicates that the radial expansion of the two ICMEs at Mars is weak. B_s indicates the south component of the magnetic field. The mean values of the two ICMEs' parameters are shown in Table 1.

4. SIR Events

Based on the SIRs' criteria, we identified three SIR events from 2021 November 16 to December 31. The SIR catalog and mean parameters of the SIR are shown in Table 2. During 2021 November 18–19, a SIR event (SIR-1) was recorded by the Tianwen-1 and MAVEN spacecraft as illustrated in Figure 5. The lavender-colored region in the figure shows the beginning and end times of the SIR. From November 18 13:00 UT to November 19 13:00 UT, SIR-1 lasts about 24 hr, which is shorter than the average duration of SIRs at Mars (Huang et al. 2019). During this period, the SIR-1 shows a compressed magnetic field, compressed proton number density, increased temperature, and continuously increased solar wind speed. No
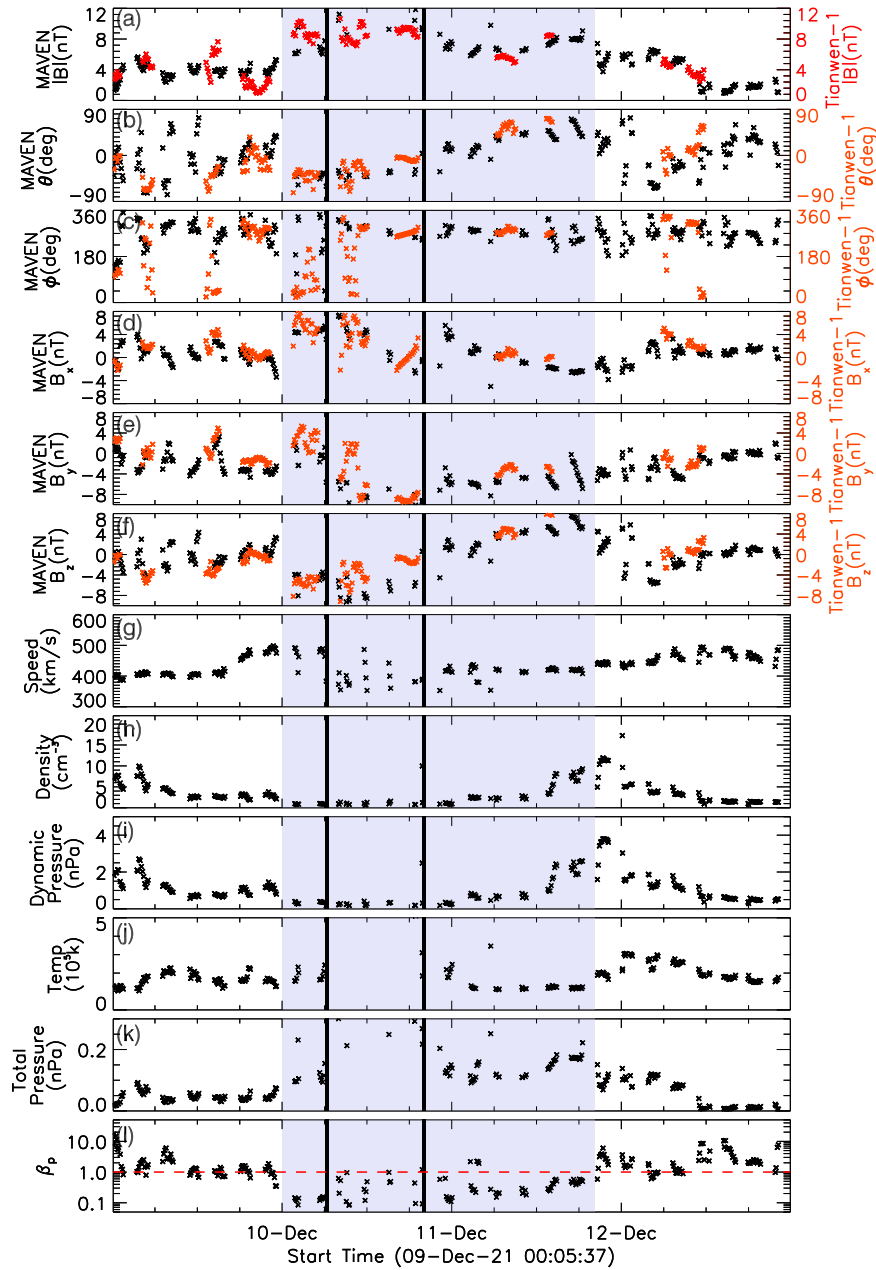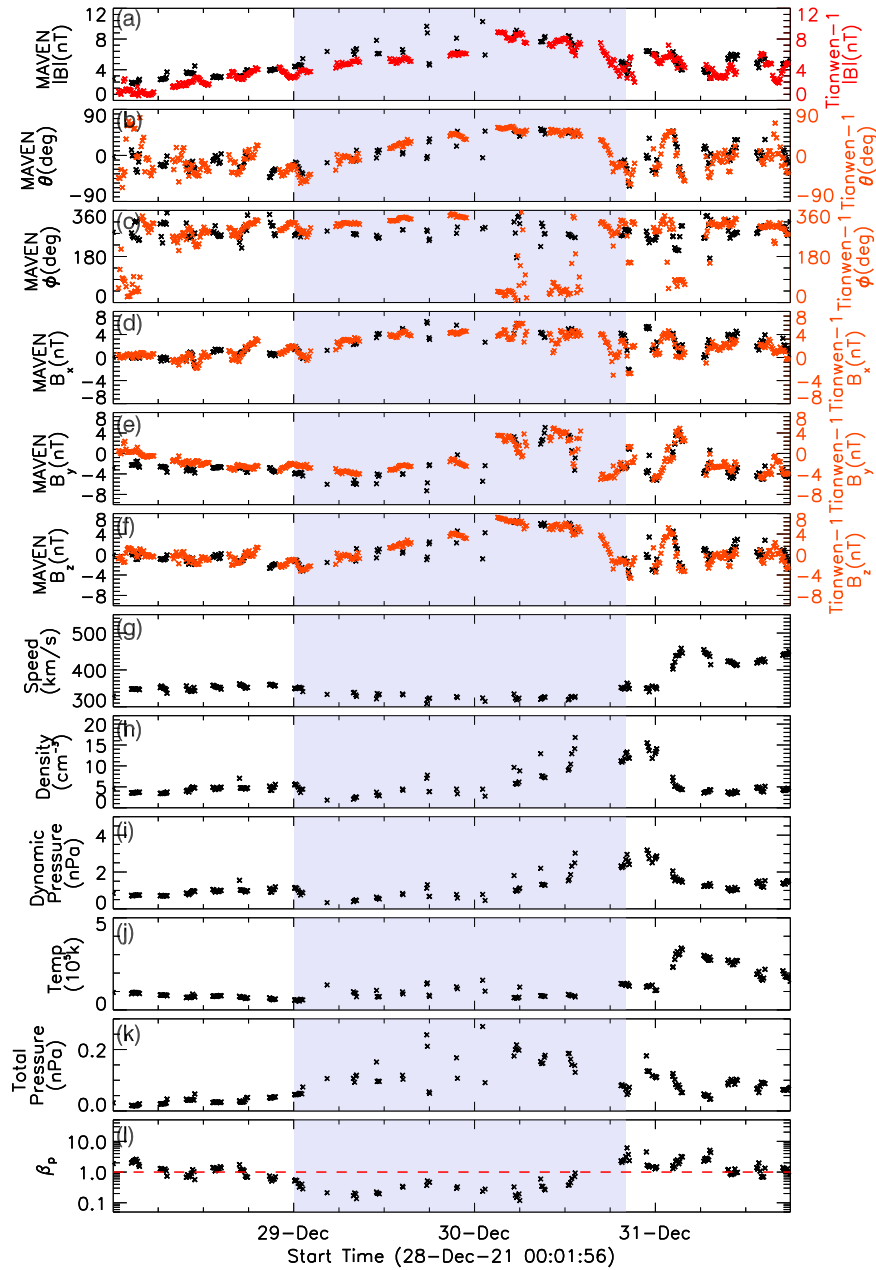
Figure 3. Tianwen-1 and MAVEN spacecraft in situ observations of a 4 day time interval starting from 00:05 UT on 2021 December 9. From top to bottom, these panels show the magnetic field strength (B), the elevation (θ), and azimuthal (ϕ) angles of the magnetic field in the MSO coordinate system; three components of the magnetic field in the MSO coordinate system (B_x, B_y, and B_z) from MAVEN/MAG (black asterisks) and Tianwen-1/MOMAG (red asterisks). Panels (g)–(l) show the solar wind speed (V_{sw}), proton density (N_p), dynamic pressure (P_{dp}), proton temperature (T_p), total pressure (P_t), and proton beta (β) from MAVEN/SWIA. The lavender-colored band indicates the interval corresponding to the ICME inferred from the data in this figure. The two vertical black lines represent the interval in which we only use three out of four criteria (neglecting the criterion of $\sqrt{(T/|v|)} < 0.012$) to select the MAVEN undisturbed solar wind periods.

clear forward or reverse shocks associated with SIR-1 are observed. The maximum magnetic field of SIR-1 is 9.5 nT. The velocity of the SIR increased from ∼390 to 518.53 km s^{-1}, with an average value of 415.04 km s^{-1}. The simultaneous decrease in proton density and increase in proton temperature can be used to identify a stream interface. The blue vertical line in Figure 5 shows the time of the stream interface at 03:40 UT on November 19, which was also identified by Su et al. (2023).

From 2021 December 16 to December 18, the Tianwen-1 and MAVEN spacecraft detected another SIR event (SIR-3). The two events (SIR-1 and SIR-3) are separated by an interval of 27.7 days, approximately corresponding to one solar rotation. As shown in Figure 6, the lavender-colored region

indicates the interval of the SIR. The interval of the SIR lasts only 23 hr, much less than the typical duration of SIRs at Mars (Huang et al. 2019). A clear forward shock is characterized by simultaneous sharp increases in magnetic field intensity, bulk velocity, proton density, and dynamic pressure at 06:00 UT on 2021 December 16. The velocity in the interval of SIR-3 increased from about 300 to 545 km s^{-1}, with an average value of 446.9 km s^{-1}. The maximum magnetic field of SIR-3 was detected by MAVEN/MAG at 9.5 nT and Tianwen-1/ MOMAG at 8.8 nT, which is a little less than the average magnetic field of SIR obtained by Huang et al. (2019). The average magnetic field intensity of SIR-3 is 4.95 nT. The maximum and mean density of SIR-3 are 20 cm^{-3} and 6.01

Figure 4. Tianwen-1 and MAVEN spacecraft in situ observations of a 4 day time interval starting from 00:01 UT on 2021 December 28. The lavender-colored band indicates the interval of an ICME inferred from the data in this figure. The plot setup is the same as in Figure 3.

Table 1
The Beginning and End Times of CMEs Detected by the Tianwen-1 Spacecraft at Mars

| No. | Shock Time | Beginning Time of the Ejecta | End Time of the Ejecta | Mean Values in the Ejecta | | | | | | |
	(UT)	(UT)	(UT)	B (nT)	B_s (nT)	V_{ejecta} (km s^{-1})	V_e (km s^{-1})	T_p (10^5 K)	N_p (cm^{-3})	P_{dp} (nPa)
1	⋯	2021-12-10T00:00	2021-12-11T14:10	7.02	4.99	438.88	1.091	1.57	1.82	0.57
2	⋯	2021-12-29T00:00	2021-12-30T20:00	6.33	1.67	335.55	0.513	0.81	6.37	1.20

cm^{-3}, respectively. Due to a lack of continuous plasma data in the solar wind, it is hard to identify the stream interface of SIR-3. The blue vertical line in Figure 6 indicates a possible stream interface for SIR-3, with increased proton temperature and decreased proton density at 19:50 UT on December 16. When comparing the two SIRs, SIR-3 has a lower magnetic field, a quicker solar wind velocity, a higher proton temperature, and a

larger plasma density than SIR-1. The similar increasing solar wind velocity trend, the magnetic field intensity, and the 27 day gap in arrival time indicate that these two fast solar wind streams are from the same coronal hole and are observed in two adjacent solar rotations.

As shown in Figure 7, the lavender-colored region shows the interval of SIR-2 detected by the Tianwen-1 and MAVEN

Table 2
The Beginning and End Times of SIRs Detected by the Tianwen-1 Spacecraft at Mars

No.	Beginning Time of the SIR (UT)	End Time of the SIR (UT)	Time of Stream Interface (UT)	Mean Values in the SIR					
				B (nT)	B_s (nT)	V_{sw} (km s^{-1})	T_p (10^5 K)	N_p (cm^{-3})	P_{dp} (nPa)
1	2021-11-18T13:00	2021-11-19T13:00	2021-11-18T18:30	5.33	2.12	415.04	1.90	5.73	1.62
2	2021-12-2T11:00	2021-12-3T19:30	2021-12-3T15:30	9.06	2.93	428.47	2.24	9.33	2.61
3	2021-12-16T06:00	2021-12-17T04:00	2021-12-16T19:40	4.95	1.80	446.95	2.26	6.01	1.78
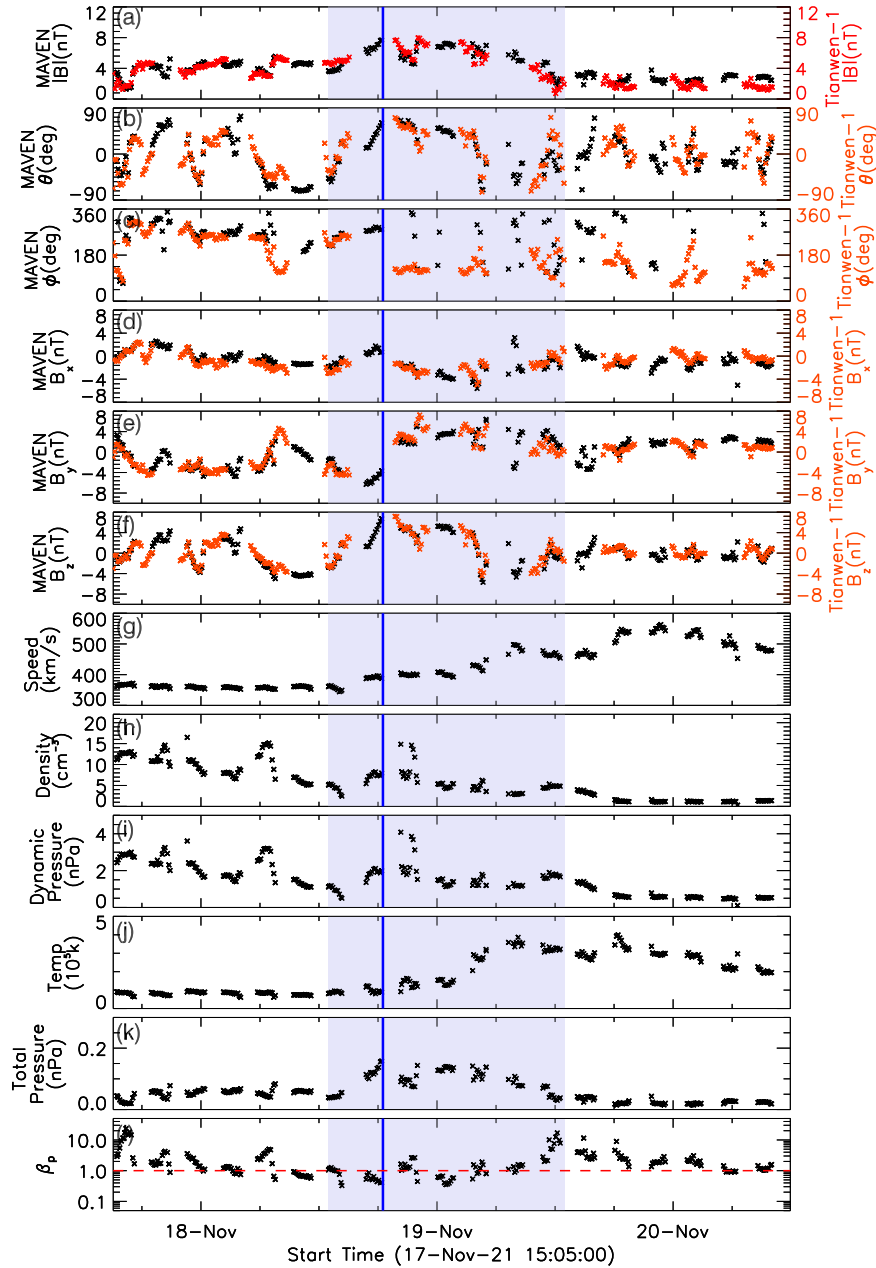
Figure 5. Tianwen-1 and MAVEN in situ observations of a 3 day time interval starting from 15:05 UT on 2021 November 17. The lavender-colored band indicates the SIR interval from the data in this figure. The blue vertical line indicates the stream interface of the SIR. The plot setup is the same as in Figure 3.

spacecraft. A pair of forward–reverse shocks bounding SIR-2 are observed at about 11:00 UT on December 2 and 19:30 UT on December 3, respectively. The forward shock is identified by the simultaneous increase in the magnetic field, bulb velocity, proton density, and dynamic pressure. The characteristics of reverse shock are a sharp increase in bulk velocity, and

a decrease in the magnetic field, proton density, and dynamic pressure. It should be noted that only approximately 4% of SIRs are associated with the forward–reverse shock pair (Huang et al. 2019) at Mars. SIR-2 lasts about 32.5 hr, which is comparable to the average duration of SIRs on Mars. The velocity of SIR-2 increased from ∼300 to 581.02 km s^{-1}, with
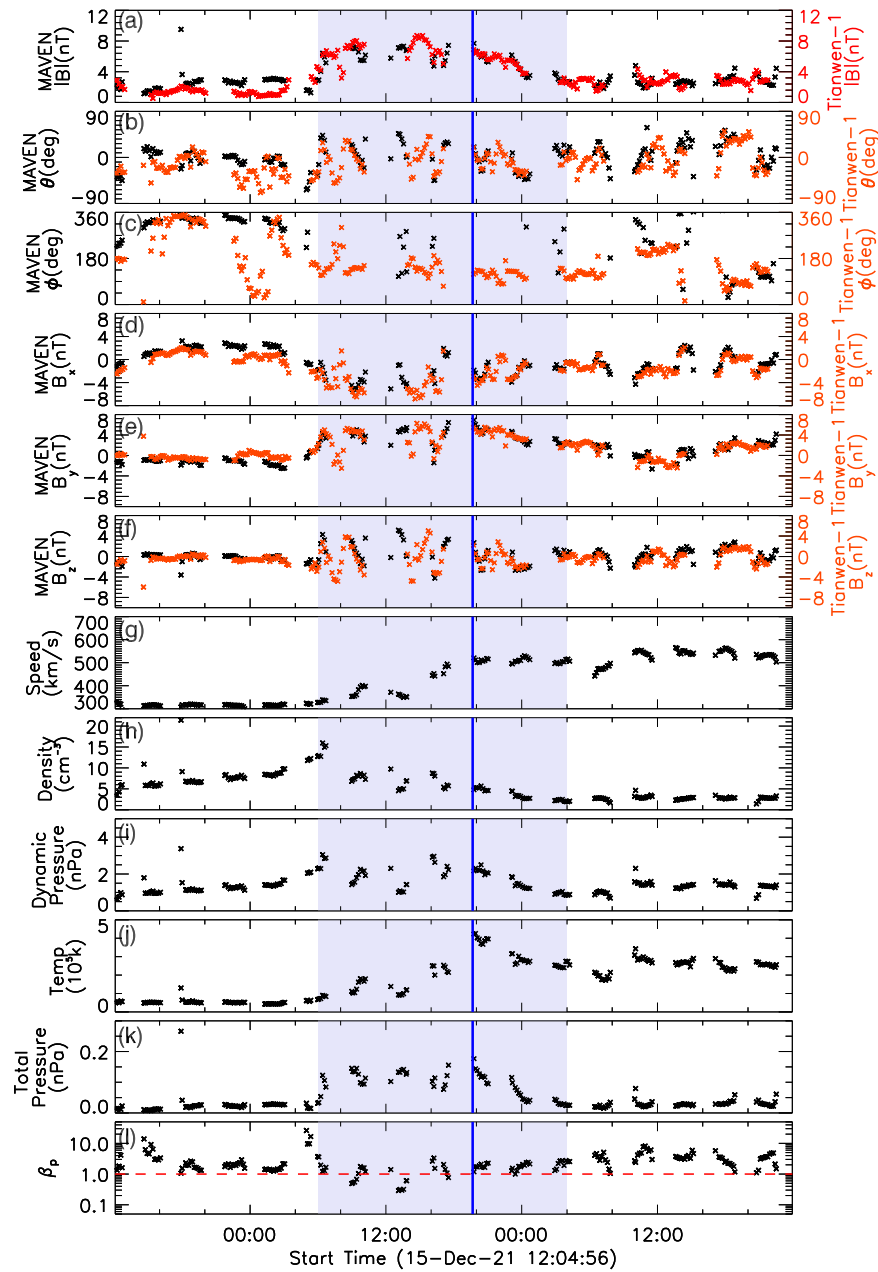
Figure 6. Tianwen-1 and MAVEN spacecraft in situ observations of a 3 day time interval starting from 12:04 UT on 2021 December 15. The lavender-colored band indicates the SIR interval inferred from the data in this figure. The plot setup is the same as in Figure 3.

an average value of 428.47 km s^{-1}. The mean magnetic field of SIR-2 is 9.06 nT, showing a significant enhancement over the surrounding solar wind.

If the SIR rotates following the solar rotation, one more SIR should be detected by Tianwen-1 and MAVEN 27 days after SIR-2. We surveyed the in situ observations from Tianwen-1 and MAVEN in the period of 2021 December 28–31. Only one typical ICME was recorded during that time, as shown in Figure 4. After the interval of ICME-2, a clear increase in bulk velocity and temperature, and a decrease in proton density and pressure, are shown in Figure 4. It indicates that the structure would be composed of an SIR and an ICME or complex ejecta. Figure 1 shows the positions of Mars, Venus, Mercury, and Earth. We will research the evolution of SIRs from 1 to 1.52 au and predict the arrival time of SIRs (Chi et al. 2022) in the future by combining in situ observations from the Wind

spacecraft close to Earth and the STEREO-A spacecraft with the SIR catalog (Jian et al. 2006; Chi et al. 2018).

5. Conclusions and Discussions

The Tianwen-1 mission is China's first Mars exploration mission. The MOMAG on Tianwen-1 can make high-quality measurements of the vector magnetic field in near-Mars space. The magnetic field data between 2021 November 16 and December 31 from MOMAG have been released to the public recently. We present ICME and SIR lists using the first available magnetic field measurements from Tianwen-1/MOMAG, as well as the observations from MAVEN/MAG and SWIA.

The magnetic field observations from MOMAG and MAG provide a unique opportunity to jointly measure and compare
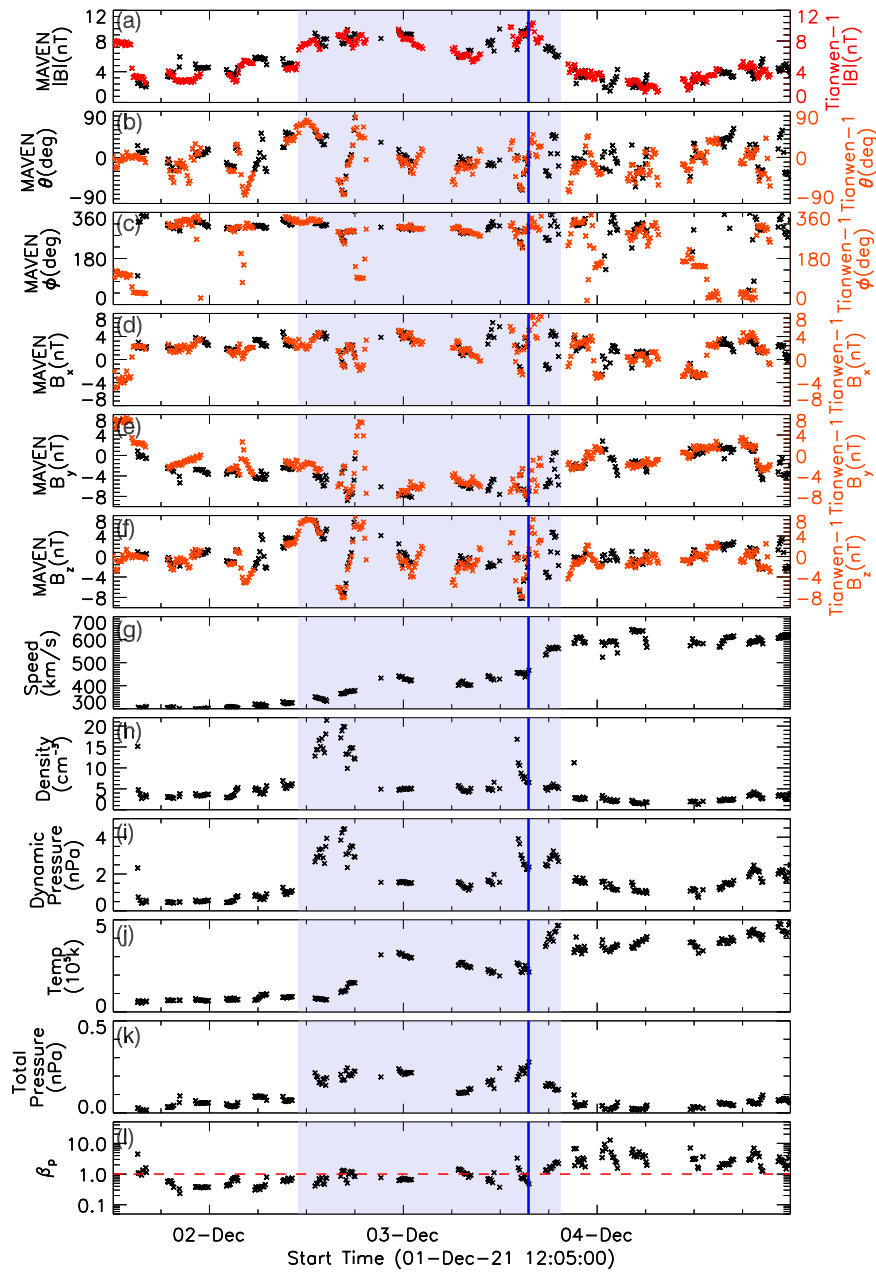
Figure 7. Tianwen-1 and MAVEN spacecraft in situ observations of a 4 day time interval starting from 12:05 UT on 2021 December 1. The lavender-colored band indicates the interval of an SIR inferred from the data in this figure. The plot setup is the same as in Figure 3.

the vector magnetic field in the interval of ICMEs and SIRs. As we presented in the paper, the total magnetic field intensity, the elevation (θ) and azimuthal (ϕ) components of magnetic field direction, and the three components of the magnetic field (B_x, B_y, and B_z) in the MSO coordinates measured by Tianwen-1/MOMAG are comparable to the observations from MAVEN/MAG. Given that MAVEN altered its orbit and shortened its time in the solar wind in 2019, the Tianwen-1/MOMAG data is currently the only interplanetary magnetic field monitor at Mars. We are looking forward to further studies of ICMEs and SIRs near Mars using multiple observations from Tianwen-1 and MAVEN. Those observations can advance our understanding of the characteristics of SIRs and ICMEs near Mars.

In the future, the multipoint observations combining BepiColombo, STEREO, Wind, Solar and Heliospheric Observatory, Tianwen-1, and MAVEN will provide a unique

opportunity to address the origin and propagation of ICMEs from the solar surface to 1.52 au. As shown in Figure 1, during that time these spacecraft have the chance to be in alignment (conjunction), which will help us to address some of the unresolved issues of CME evolution in the heliosphere. It also provides us a chance to investigate the evolution of SIR basic properties and related shocks from 1 au to 1.52 au, when combined with measurements from Wind or STEREO-A at 1 au. The arrival of ICMEs and SIRs can disrupt the entire Martian upper atmosphere–ionosphere–magnetosphere system and have a significant impact on the instantaneous rates of ion loss in the Martian atmosphere (Jakosky et al. 2015b). The Mars Ion and Neutral Particle Analyzer (MINPA; Kong et al. 2020) and the Mars Energetic Particles Analyzer (MEPA; Tang et al. 2020) on board Tianwen-1 can detect low-energy ions, neutral particles, electrons, protons, alpha particles, and heavy

ions in the space plasma environment of Mars. The observations from MOMAG, MINPA, and MEPA on board the Tianwen-1 spacecraft will show the response of the Martian upper atmosphere–ionosphere–magnetosphere system to ICMEs or SIRs.

ORCID iDs

Yutian Chi ⬭ https://orcid.org/0000-0001-9315-4487
Chenglong Shen ⬭ https://orcid.org/0000-0002-3577-5223
Long Cheng ⬭ https://orcid.org/0000-0003-0578-6244
Bingkun Yu ⬭ https://orcid.org/0000-0003-2758-1960
Yuming Wang ⬭ https://orcid.org/0000-0002-8887-3919
Zhuxuan Zou ⬭ https://orcid.org/0009-0008-9920-9600
Mengjiao Xu ⬭ https://orcid.org/0000-0002-2924-7520
Zhenpeng Su ⬭ https://orcid.org/0000-0001-5577-4538
Zhihui Zhong ⬭ https://orcid.org/0000-0002-5627-2377
Junyan Liu ⬭ https://orcid.org/0009-0006-7051-0438
Guoqiang Wang ⬭ https://orcid.org/0000-0002-6618-4928
Kai Liu ⬭ https://orcid.org/0000-0003-2573-1531

References

Brain, D. A., McFadden, J., Halekas, J. S., et al. 2015, GeoRL, 42, 9142

Burlaga, L., Sittler, E., Mariani, F., & Schwenn, A. R. 1981, JGR, 86, 6673
Cannon, P., Angling, M., Barclay, L., et al. 2013, Extreme Space Weather: Impacts on Engineered Systems and Infrastructure, (London: Royal Academy of Engineering) https://raeng.org.uk/media/lz2fs5ql/space_weather_full_report_final.pdf
Chi, Y., Shen, C., Luo, B., Wang, Y., & Xu, M. 2018, SpWea, 16, 1960
Chi, Y., Shen, C., Scott, C., et al. 2022, SpWea, 20, e2022SW003112
Chi, Y., Shen, C., Wang, Y., et al. 2016, SoPh, 291, 2419
Connerney, J., Espley, J., Lawton, P., et al. 2015a, SSRv, 195, 257
Connerney, J. E., Espley, J. R., DiBraccio, G. A., et al. 2015b, GeoRL, 42, 8819
Crider, D. H., Espley, J., Brain, D. A., et al. 2005, JGRA, 110, A09S21
Dubinin, E., Fraenz, M., Woch, J., et al. 2009, GeoRL, 36, L01105
Gonzalez, W. D., Tsurutani, B. T., & De Gonzalez, A. L. C. 1999, SSRv, 88, 529
Gosling, J., & Pizzo, V. 1999, in Corotating Interaction Regions, ed. A. Balogh et al. (Dordrecht: Springer Netherlands), 21
Halekas, J., Ruhunusiri, S., Harada, Y., et al. 2017, JGRA, 122, 547
Halekas, J., Taylor, E., Dalton, G., et al. 2015, SSRv, 195, 125
Huang, H., Guo, J., Wang, Z., et al. 2019, ApJ, 879, 118
Jakosky, B. M., Grebowsky, J. M., Luhmann, J. G., et al. 2015b, Sci, 350, 0210
Jakosky, B. M., Lin, R. P., Grebowsky, J. M., et al. 2015a, SSRv, 195, 3
Jian, L., Russell, C., Luhmann, J., & Skoug, R. 2006, SoPh, 239, 337
Kong, L., Zhang, A., Tian, Z., et al. 2020, E&PP, 4, 333
Liu, K., Hao, X., Li, Y., et al. 2020, E&PP, 4, 384
Morgan, D. D., Gurnett, D. A., Kirchner, D. L., et al. 2010, Icar, 206, 95
Richardson, I. G., & Cane, H. V. 2012, JSWSC, 2, A01
Rouillard, A., & Lockwood, M. 2007, AdSpR, 40, 1078
Shen, C., Chi, Y., Wang, Y., Xu, M., & Wang, S. 2017, JGRA, 122, 5931
Su, Z., Wang, Y., Zhang, T., et al. 2023, ApJL, 947, L33
Tang, S., Wang, Y., Zhao, H., et al. 2020, E&PP, 4, 355
Trotignon, J., Mazelle, C., Bertucci, C., & Acuña, M. 2006, P&SS, 54, 357
Wan, W., Wang, C., Li, C., & Wei, Y. 2020, NatAs, 4, 721
Wang, C., Rosen, I. G., Tsurutani, B. T., et al. 2016, JSWSC, 6, A5
Wang, Y., Zhang, T., Wang, G., et al. 2023, E&PP, 7, 1
Wang, Y., Zhou, Z., Shen, C., Liu, R., & Wang, S. 2015, JGRA, 120, 1543
Xu, S., Fang, X., Mitchell, D. L., et al. 2018, GeoRL, 45, 7337
Yiğit, E., Knížová, P. K., Georgieva, K., & Ward, W. 2016, JASTP, 141, 1
Yu, B., Scott, C. J., Xue, X., et al. 2021, ApJ, 916, 106
Zhang, C., Rong, Z., Nilsson, H., et al. 2021a, ApJL, 922, L33
Zhang, J., Richardson, I., Webb, D., et al. 2007, JGRA, 112, A10102
Zhang, J., Temmer, M., Gopalswamy, N., et al. 2021b, PEPS, 8, 56
Zhao, D., Guo, J., Huang, H., et al. 2021, ApJ, 923, 4
Zou, Z., Wang, Y., Zhang, T., et al. 2023, Sci. China Tech. Sci., in press (arXiv:2302.04671)